Annual forest maps in the contiguous United States during 2015-2017 from analyses of PALSAR-2 and Landsat images

Jie Wang[1,*], Xiangming Xiao[2,*], Yuanwei Qin[2], Jinwei Dong[3], Geli Zhang[4], Xuebin Yang[2], Xiaocui Wu[5],

Chandrashekhar Biradar[6], Yang Hu[7]

[1] College of Grassland Science and Technology, China Agricultural University, Beijing 100093, China

[2] School of Biological Sciences~~Department of Microbiology and Plant Biology~~, Center for Earth Observation

and Modeling, University of Oklahoma, Norman, OK 73019, USA

[3] Key Laboratory of Land Surface Pattern and Simulation, Institute of Geographic Sciences and Natural

Resources Research, Chinese Academy of Sciences, Beijing 100101, China

[4] College of Land Science and Technology, China Agricultural University, Beijing 100193, China

[5] Department of Natural Resources and Environmental Sciences, University of Illinois at Urbana-Champaign,

Urbana, IL 61801, USA

[6] Center for International Forestry Research (CIFOR) and World Agroforestry Center (ICRAF), Asia Continental

Program, New Delhi, India

[7] School of Ecology and Environment, Ningxia University, Yinchuan 750021, China

Corresponding author: Xiangming Xiao, Ph.D. (xiangming.xiao@ou.edu)

School of Biological Sciences~~Department of Microbiology and Plant Biology~~, University of Oklahoma

101 David L. Boren Blvd., Norman, Oklahoma 73019-5300, USA

~~Phone: (405) 325-8941;~~

~~Website: http://www.ceom.ou.edu~~

Jie Wang, Ph.D. (jiewang178@cau.edu.cn)

College of Grassland Science and Technology, China Agricultural University

Yuanmingyuan West Road 2, Beijing 100193, China

Abstract: Annual forest maps at a high spatial resolution are necessary for forest management and conservation. Large uncertainties remain among the existing forest maps, because of different forest definitions, satellite datasets, in-situ training datasets, and mapping algorithms. In this study, we generated annual forest maps and evergreen forest maps at a 30-m resolution in the Contiguous United States (CONUS) during 2015-2017 by integrating microwave data (Phased Array type L-band Synthetic Aperture Radar (PALSAR-2)) and optical data (Landsat) using Knowledge-based algorithms. The resultant PALSAR-2/Landsat-based forest maps (PL-Forest) were compared with five major forest datasets in the CONUS: (1) the Landsat tree canopy cover from Global Forest Watch datasets (GFW-Forest), (2) the Landsat Vegetation Continuous Field datasets (Landsat VCF-Forest), (3) the National Land Cover Database 2016 (NLCD-Forest), (4) the Japan Aerospace Exploration Agency (JAXA) forest maps (JAXA-Forest), and (5) the Forest Inventory and Analysis (FIA) data from the USDA Forest Service (FIA-Forest). The forest structure data (tree canopy height and canopy coverage) derived from the lidar observations of the Geoscience Laser Altimetry System (GLAS) onboard of NASA's Ice, Cloud, and land Elevation Satellite (ICESat-1) were used to assess the five forest datasets derived from satellite images. Using the forest definition by the Food and Agricultural Organization (FAO) of the United Nations, more forest pixels from the PL-Forest maps meet the FAO's forest definitions than the GFW-, Landsat VCF-, and JAXA-Forest datasets. Forest area estimates from the PL-Forest were close to those from the FIA-Forest statistics but higher than the GFW-Forest, NLCD-Forest and lower than the Landsat VCF-Forest, which highlights the potential of using both PL-Forest and FIA-Forest datasets to support the FAO's Global Forest Resources Assessment. Furthermore, the PL-based annual evergreen forest maps (PL-Evergreen Forest) showed reasonable consistency with the NLCD product. Together with our previous work in South America and monsoon Asia, this study further demonstrates the potential of integrating PALSAR and Landsat images for developing annual forest maps and forest-type maps at high spatial resolution across the scales from region to the globe, which could be used to support FAO's Global Forest Resources Assessments. The PL-Forest and PL-Evergreen Forest datasets are publicly available at https://doi.org/10.6084/m9.figshare.21270261 (Wang et al., 2022).

Keywords: Forest map, Tree canopy height, Tree canopy cover, Evergreen Forest, Deciduous Forest

1 Introduction

Forests cover approximately 30% of the land surface and have played major roles on regulating terrestrial carbon and water cycles (D'Almeida et al. 2007; Harris et al. 2012), influencing climate (Bonan 2008; Peng et al. 2014), conserving biodiversity (Betts et al. 2017; Seto et al. 2012), and supplying forest products to humankinds (Foley et al. 2005; Smith et al. 2018). The United States of America is covered by 310 million hectares of forests, which is the fourth largest forest country in the world, as estimated in 2020 (Global Forest Resources Assessment 2020). The forest inventory and analysis (FIA) program, managed by the USDA Forest Service, reported that the national forest area totals remain stable, but substantial changes occurred at regional and local scales (Oswalt; et al. 2019). In addition, extensive impacts of disturbance (e.g., wildfires, harvests, insect outbreaks) and climate factors have been increasingly changing the forest structure, function, and species composition (Mekonnen et al. 2019; Sexton et al. 2016). To identify the forest dynamics and assessing the associated impacts more effectively, it is critical to generate timely and accurate annual forest maps at a high spatial resolution to support policy decisions and relevant research (Sexton et al. 2015).

Remote sensing technology offers large-area and high-frequency observations that have been widely used for continental and global forest mapping. For example, the optical-based regional and global forest maps are generated at the coarse (thousands of meters) and moderate (hundreds of meters) spatial resolutions using the 1-km Advanced Very High Resolution Radiometer (AVHRR) (Achard et al. 2001; Hansen and DeFries 2004), 1-km Satellite Pour I'Observation de Ia Terre 4 (SPOT-4) VEGETATION (Souza et al. 2003; Stibig and Malingreau 2003; Stibig et al. 2004), and 250-m and 500-m Moderate Resolution Imaging Spectroradiometer (MODIS) (DiMiceli et al. 2017; Friedl et al. 2010; Hansen et al. 2003). The characteristics and comparisons of several major forest cover products at the moderate spatial resolution have been shown in detail in one of our previous studies, including image data sources, forest definition, algorithms, accuracy and other relevant information (Qin et al. 2017).

The Landsat images have been used to generate forest or other land cover products at a high spatial resolution (tens of meters) (Chen et al. 2015; Hansen et al. 2013a; Jin et al. 2013a). The major Landsat-based products for the CONUS include the Global Forest Watch (GFW) program of the World Resources Institute (2013b), the forest cover fraction (VCF) product from the Global Land Cover Facility Data Center (GLCF) at the University of Maryland (Sexton et al. 2013b), and the National Land Cover Database (NLCD) from USGS (Jin et al. 2013b). In the United States, FIA and NLCD are the primary databases used by managers, researchers, and policymakers to assess land use

80   and track land management (Domke et al. 2021; Hoover et al. 2020). FIA is a field survey of forest plots and reports information on the status and trends of forests in the United States. A subset of plots is measured every year with revisit intervals of 5 to 10 years depending on the state (Burrill et al. 2021; Hoover et al. 2020). The NLCD provides updated datasets continuously every about three years or so, which was generated by change detection algorithms for only a time period and had a certain amount of commission errors (Jin et al. 2013a). Additionally, the annual global

85   forest maps have been published by JAXA over the years of 2007-2010 and 2015-2018, which are generated using PALSAR and PALSAR-2 images at 25-m and 50-m spatial resolutions (Shimada et al. 2014). The main characteristics of these high-spatial-resolution forest maps covering the CONUS are summarized in Table 1. However, it remains untested about their application potential for the annual management of forest resources systematically. It is noticed that the high-spatial-resolution forest maps are relatively few for the years after 2010.

90   Due to the differences in forest definitions, satellite data, in-situ training data, and mapping algorithms, the previous forest maps have large discrepancies on forest area estimates (Qin et al. 2017; Sexton et al. 2016; Smith et al. 2018). The major challenge of the optical remote sensing approach is to collect good-quality observation data without cloud cover (Reiche et al. 2015). The PALSAR-based forest maps often have commission errors caused by buildings, rocks, and high biomass crops (Qin et al. 2017). The combination of the optical and microwave data could

95   take advantage of the optical remote sensing sensors that capture the light and forest canopy interaction and microwave sensors that capture the microwave and forest structure (tree trunk and branch) interaction without cloud contamination. Additionally, an assessment study suggested that the complementarity of optical and SAR datasets improved the discriminative properties for forest mapping compared to the individual dataset (Lehmann et al. 2015). For example, uncertainties of Landsat-based forest maps could be caused by the re-planted areas with small- or medium-size trees

100 or regions with some vegetation types like highland scrub. These regions could be identified correctly by PALSAR data (Lehmann et al. 2015). Improved fForest mappings have been reportedgenerated in a number of studies by using integrated PALSAR and Landsat data in tropical regions (Lehmann et al. 2015; Reiche et al. 2015; Thapa et al. 2014), and PALSAR and MODIS data in monsoon Asia and several sample regions of the word (Qin et al. 2016b; Zhang et al. 2019). However, it remains unclear about the potential to improve the annual forest monitoring in the CONUS To

105 date, no study has by combininged PALSAR and Landsat images during 2015-2017 to map annual forest distributions in the CONUS.

In addition to annual forest maps, information on evergreen forests and deciduous forests is also important for forest management and conservation. Many studies showed that the spatial distributions of evergreen and deciduous forests have been changing and will continue to change in the future, driven by multiple stressors involving climate change, forest disturbance, land-use change, and invasive species (Knott et al. 2019; Mekonnen et al. 2019; Soh et al. 2019). Accurate distribution information of evergreen and deciduous forests types is also needed to reduce the uncertainty in the carbon budgets (Deb Burman et al. 2021). With the development of Earth observation technology, some efforts have been carried out to produce forest type datasets based on multiple spaceborne or/and airborne images (Kushwaha 1990; Laurin et al. 2016). As an example, for the study at the national or continental scale, the NLCD dataset provides the nationwide distribution of deciduous, evergreen, and mixed forests in the U.S. at 30-m spatial resolution for the years of 2001, 2006, 2011, and 2016. The 50-m evergreen and deciduous forest map in 2010 was generated across the monsoon Asia using PALSAR and time series MODIS images (Qin et al. 2016b). In addition, time series MODIS images have been reported to improve the estimates of evergreen forests in tropical regions (Qin et al. 2019). As the NLCD used multi-temporal Landsat images to identify evergreen and deciduous forests, there is a need to explore the potential of time series Landsat images could for improveing the discrimination and classification of evergreen and deciduous forests to, which could support the annual analyses in the scientific research and policy making on forest ecosystems. To date, few efforts have been conducted to explore the potential over the temperate regions despite of the importance.

The United Nations Food and Agriculture Organization (FAO) Global Forest Resources Assessment (FRA) provides essential information for understanding the world's forest resources, management and uses every five years since 1990 by assembling the forest data from individual countries (Keenan et al. 2015). In an effort to improve annual forest maps at a national scale for supporting the FAO FRA program, this study had three objectives. The first objective was to develop annual forest maps and annual evergreen forest maps in the CONUS by using both PALSAR-2 and Landsat images during 2015-2017. The second objective was to assess and compare the resultant PALSAR-2/Landsat-based forest maps with the major satellite-based forest cover datasets by using the forest structure data (tree height and tree canopy coverage), which were derived from the observations of the Geoscience Laser Altimetry System (GLAS) onboard of NASA's Ice, Cloud, and land Elevation Satellite (ICESat-1). This comparison with a large amount of LiDAR data will help understand the differences of the forest datasets under the forest definition used by the FAO. The FAO defines forest as natural forest area larger than 0.5ha with tree cover over 10% and tree height greater than

135 5-m (FAO 2012). The third objective was to report the PALSAR-2/Landsat-based forest maps at two administration levels (state and CONUS) and compare them with the forest area estimates from the Forest Inventory Assessment by the USDA Forest Service, which are the primary data sources provided by the USA government for the FAO Global Forest Resources Assessment. This comparison will help us to investigate the capability of combining the PALSAR-2/Landsat approach and the FIA approach for support of the Global Forest Resource Assessment at the national scale.

140 Table 1. Characteristics of the main forest cover datasets at a high spatial resolution (tens of meters) for the Contiguous United States.

Sensors	Datasets	Forest definition	Major data source	Methods	Spatial resolutions	Periods	References
Statistics	FIA	Tree cover≥10%	Inventory data	Sampling	State	Annual sampling design after 1998	Burrill et al. (2021)
Optical	NLCD	Tree cover≥ 20%, tree height ≥ 5-m	Landsat images	Decision tree	30-m	circa 1992, 2001, 2006, 2011, 2016, 2019	Jin et al. (2019)
	Landsat VCF	tree height ≥ 5-m	MODIS VCF, Landsat images	Regression tree	30-m	2000, 2005, 2010, 2015	Sexton et al. (2013a)
	GFW	tree height ≥ 5-m	Landsat images	Decision tree	30-m	2000, 2010	Hansen et al. (2013a)
SAR	JAXA	Tree cover ≥ 10%, tree height ≥ 5-m	PALSAR/PALSAR-2 images	Decision tree	25-m	2007-2010, 2015-2018	Shimada et al. (2014)
SAR/Optical	PL-Forests	Tree cover ≥ 10%, tree height ≥ 5-m	25-m PALSAR-2 and 30-m Landsat images in 2015-2017	Decision tree	30-m	2015-2017	This study

2 Materials and Methods

The workflow in Fig. 1 presents the three major study sections and the detailed processes of each section in this
145 study. First, we generated the annual forest maps, annual evergreen and deciduous forest maps at 30-m spatial resolution during 2015-2017 by integrating PALSAR-2 and Landsat time-series NDVI data. Second, we compared the resultant PALSAR-2/Landsat forest maps with other major satellite-based forest datasets in the study period of 2015-2017. We assessed these forest maps following the FAO's forest definition using the tree height and canopy coverage data from the ICESat-1 LiDAR-based products. Third, we examined the performance all the satellite-based

150 forest maps on forest area estimates by comparison with the FIA statistic data at the state and national administration

levels.
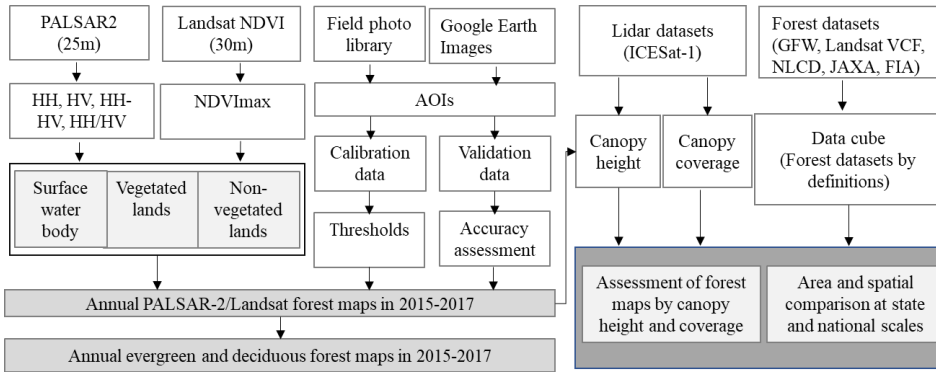
Figure 1: The workflow of this study. It includes three major study sections and the detailed processes of each section in this study.

155 **2.1 Study area**

Our study area is the CONUS with an area of about 8.08×10^6 km^2, including the 48 states and Washington, DC.

About 50% of the CONUS land cover change has involved forests since 2001(Homer et al. 2020). The CONUS has

large topographical variation from the eastern USA to the western USA as shown by the spatial distribution of

topography in the CONUS (Fig. 2).
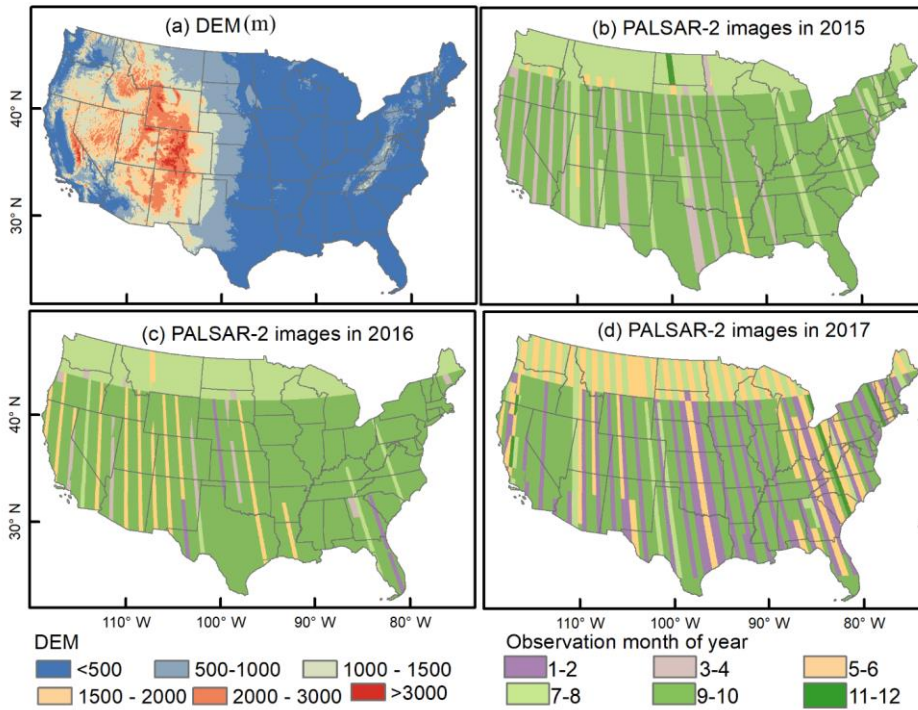
Figure 2: The spatial distributions of (a) the topography of the CONUS using the digital elevation model (DEM). (b, c, d) the acquisition dates of PALSAR-2 images in a year during 2015 - 2017.

2.2 PALSAR-2 data in 2015-2017

      The annual 25-m ALOS-2 PALSAR-2 mosaic data from 2015 to 2017 were collected at the Google Earth Engine (GEE) platform (https://developers.google.com/earth-engine/datasets/catalog/JAXA_ALOS_PALSAR_YEARLY_SAR, last access: 18 March 2022). The PALSAR-2 HH and HV polarization bands, provided by the Earth Observation Research Center, Japan Aerospace Exploration Agency (JAXA), are slope corrected, radiometrically calibrated, and ortho-rectified backscatters with a geometric accuracy of around 12 meters (Reiche et al. 2018). Fig. 2 shows the acquisition dates of the PALSAR-2 mosaic images over the CONUS and most images were acquired during May to October. The HH and HV bands were converted from the amplitude values into gamma-naught backscattering coefficients in decibels ($\gamma°$) using a calibration factor (CF) of -83

($\gamma°=10\times ln\text{DN}^2 + \text{CF}$). Two composite layers, i.e., the difference (HH-HV) and the ratio (HH/HV), were calculated as input data for forest mapping.

2.3 Landsat data in 2015-2017

175   We used all the Landsat-7 Enhanced Thematic Mapper (ETM+) and Landsat-8 Operational Land Imager (OLI) surface reflectance (SR) images from 2015 to 2017 to construct a time series image data cube in GEE (https://developers.google.com/earth-engine/datasets/catalog/LANDSAT, last access: 18 March 2022). This dataset provides multi-spectral images at 30-m resolution and the SR data were derived from top of atmosphere (TOA) reflectance by the atmospheric correction codes (Vermote et al. 2016). The bad-quality observations with clouds,

180   cloud shadows, snow/ice, and scan-line-off strips were identified as NODATA following the quality band (pixel_qa). The remaining good-quality observations were used to calculate the vegetation indices of NDVI, EVI, and LSWI for each image in the data cube. Fig. 3 shows the spatial distribution of annual total good-quality observation numbers (GOBs) for individual pixels over the CONUS from 2015 to 2017.

$$NDVI = \frac{\rho_{NIR}-\rho_{Red}}{\rho_{NIR}+\rho_{Red}} \tag{1}$$

185

$$EVI = 2.5 \times \frac{\rho_{NIR}-\rho_{Red}}{\rho_{NIR}+6\times\rho_{Red}-7.5\times\rho_{Blue}+1} \tag{2}$$

$$LSWI = \frac{\rho_{NIR}-\rho_{SWIR}}{\rho_{NIR}+\rho_{SWIR}} \tag{3}$$

where ρ_{Blue}, ρ_{Red} ρ_{NIR} and ρ_{SWIR} are the surface reflectance values of blue (450-520nm), red (630-690nm), near-infrared (760-900nm), and shortwave-infrared bands (1550-1750nm).
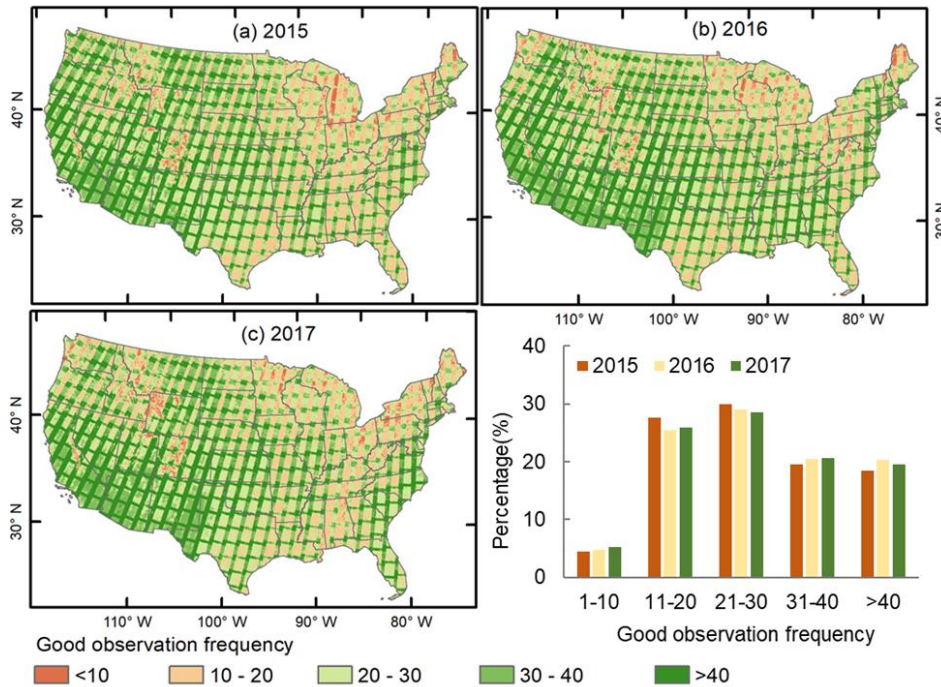
Figure 3: The summary of the good-quality observation (GOBs) numbers for individual pixels in a year over the CONUS using all Landsat images in a year during 2015-2017.

2.4 Sample data for accuracy assessment of forest maps

The accuracy of the PALSAR-2/Landsat annual forest maps were assessed based on the global validation sample set released by researchers from Tsinghua University, China (http://data.ess.tsinghua.edu.cn/, last access: 20 February 2022) (Gong et al. 2013). This validation dataset was generated using a random sampling strategy and visual interpretation method for the Finer Resolution Observation and Monitoring-Global Land Cover (FROM-GLC) (Gong et al. 2013). The samples with land cover changes were identified visually according to the Google Earth images during 2015-2017, which were and removed out according to the Google Earth images during 2015-2017in this study. A total number of 1,958 points were used for the validation of the resultant forest maps, which includes 652 forests, 285 croplands, 431 grasslands, 205 shrublands, 95 water bodies and wetlands, 46 impervious surfaces, 244 barren lands (Fig. 4).
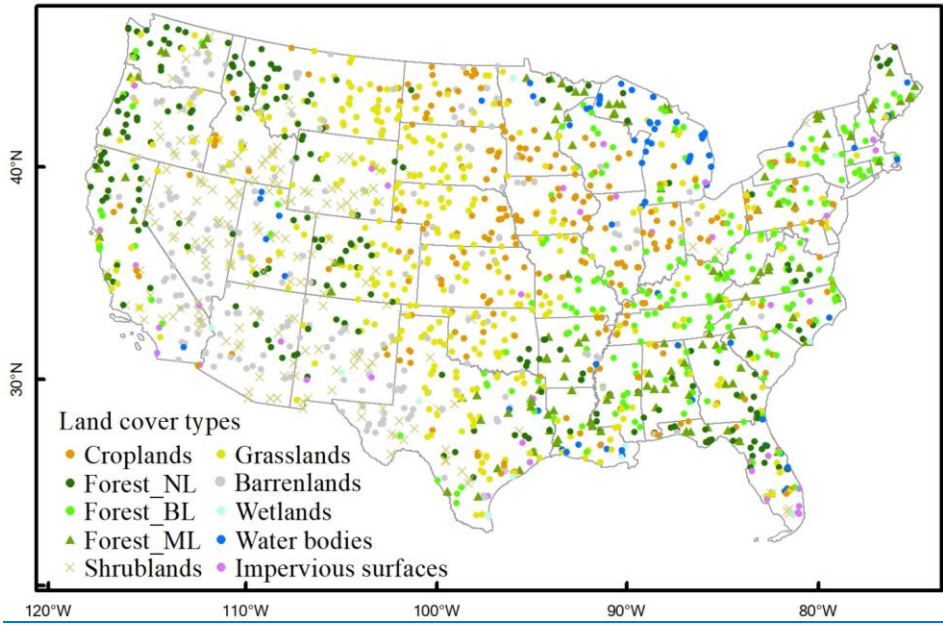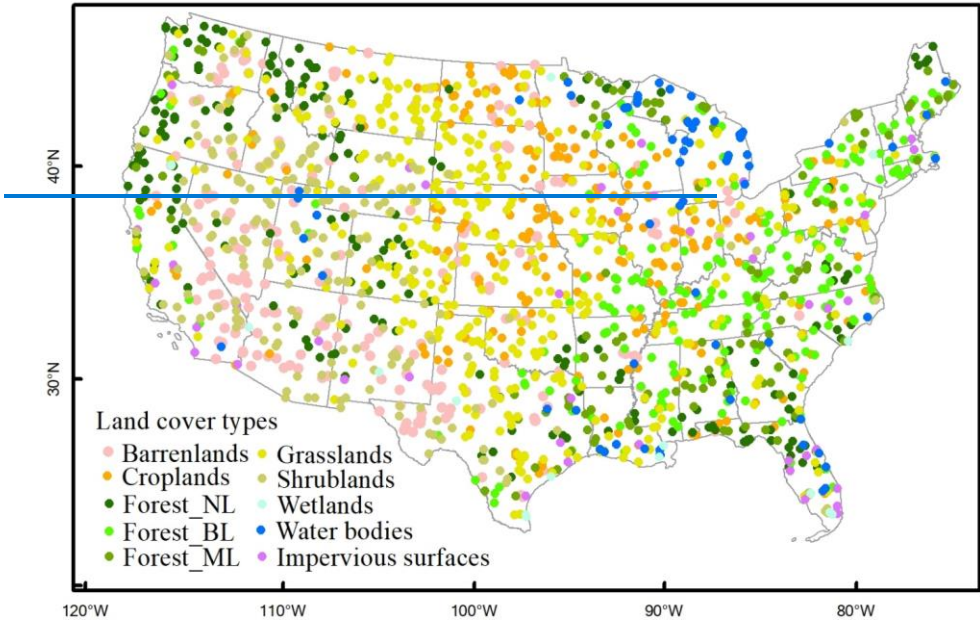
Figure 4: The land cover samples for accuracy assessment in this study. These samples were from the global validation sample set released by the third-party researchers from Tsinghua University, China (http://data.ess.tsinghua.edu.cn/) (Gong et al. 2013). They were revised by excluding the samples with land cover change according to the Google Earth images. Forest_NL, Forest_BL, and Forest_ML denote needle-leaved forest, broad-leaved forest, and mixed-leaved forest, respectively.

2.5 Canopy height and canopy coverage data from ICESat LiDAR

To assess the PALSAR-2/Landsat forest maps and other forest maps in terms of forest structure features (canopy height, canopy coverage) that are used in forest definition by FAO, we used the ICESat global canopy coverage and height dataset to generate the samples of (1) forest canopy height (meter) and (2) forest canopy coverage (%). This ICESat dataset was derived based on the observations from the Geoscience Laser Altimetry System (GLAS) on board of NASA's Ice, Cloud, and land Elevation Satellite (ICESat-1) with a footprint of about 65-m in diameter (Tang et al. 2019). The ICESat mission acquired LiDAR data over the globe during 2003-2009. The ICESat-based tree canopy cover products provide improved information to characterize biome-level gradients and canopy cover almost without bias at the foot print level (Tang et al. 2019). There are more than 550,000 laser spots from ICESat-1 over the CONUS (Fig. 5). We recognize the time difference between the ICESat data (2003-2009) and the PALSAR-2 data (2015-2017), which may affect the assessment, dependent upon the land use change. A pixel has three scenarios in terms of forest in one time-period: (1) as forest in both 2003-2009 and 2015-2017, (2) as forest in 2003-2009 but not in 2015-2017 (forest loss due to deforestation), and (3) as forest in 2015-2017 but not in 2003-2009 (forest gain due reforestation or afforestation). For those pixels that were forest in 2003-2009 and 2015-2017 (Scenario #1), as the canopy height and canopy coverage of a forest stand are likely to increase over years, there is no effect of time differences (2003-2009 vs 2015-2017) on the assessment. For those pixels with the scenario #2 and #3, the time differences could have small effect on the assessment.
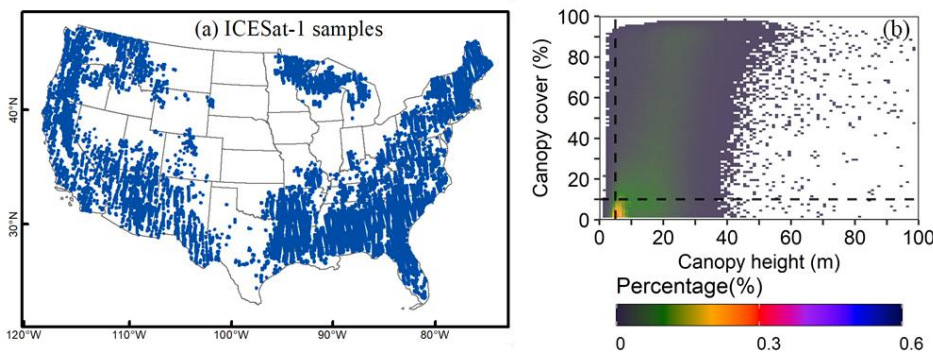
Figure 5: The ICESat samples in the CONUS, (a) Spatial distribution of ICESat-1samples. (b) the histogram of canopy height (m) and canopy coverage (%) for the ICESat-1 samples.

2.6 Five forest cover data products for inter-comparison

230   We used four forest cover products derived from analyses of satellite images at a high spatial resolution (≤30-m) for inter-comparison with our PALSAR-2/Landsat forest maps: the GFW product in 2010, the Landsat VCF product in 2015, the NLCD product in 2016 (NLCD2016), and JAXA product in 2015-2017 (Fig. 6). The GFW tree canopy cover product in 2010 at 30-m resolution was generated by using decision tree algorithms and multi-temporal Landsat images (https://www.glad.umd.edu/dataset/global-2010-tree-cover-30-m, last access: 1 May 2021) (Hansen et al.

235   2013a). The Landsat VCF product in 2015 is a global tree cover percentage dataset and can be downloaded from the Land-Cover and Land-Use Change Program (https://lcluc.umd.edu/metadata/global-30m-landsat-tree-canopy-version-4, last access: 5 May 2021). It is generated by using a regression tree model to rescale the 250-m MODIS VCF tree cover layer into 30-m (Sexton et al. 2013a). The Landsat-based NLCD2016 provides land cover information at 30-m resolution over the CONUS with an accuracy of 83% (https://www.mrlc.gov/data/nlcd-2016-land-cover-

240   conus, last access: 9 May 2021) (Homer et al. 2020). This product has three forest types: deciduous forest, evergreen forest, and mixed forest (Homer et al. 2020). The 25-m annual global forest maps from 2015 to 2017 from JAXA were produced by using thePALSAR-2 mosaic data and a decision tree method (JAXA forest maps), which are available at https://www.eorc.jaxa.jp/ALOS/en/palsar_fnf/fnf_index.html, with last access of 12 May 2021 (Shimada et al. 2014). JAXA forest used the FAO forest definition. So, similarly, for the tree cover products of Landsat VCF and GFW, we

245   selected the pixels with tree canopy coverage greater than 10% as forests.

    The forest area statistical data for year 2017 at the county scale was also used for comparison analysis. This statistical dataset comes from the USDA Forest Service (FS) Forest Inventory and Analysis (FIA) program (https://www.srs.fs.usda.gov/pubs/57903, last access: 10 May 2021) and is widely used in the studies of forests in the CONUS (Burrill et al. 2021; Domke et al. 2021; Hoover et al. 2020). It is the critical data source provided by the US

250   government for the FAO's Global Forest Resources Assessment, and for resources managers and the public to manage and utilize the forest resources in the United States.
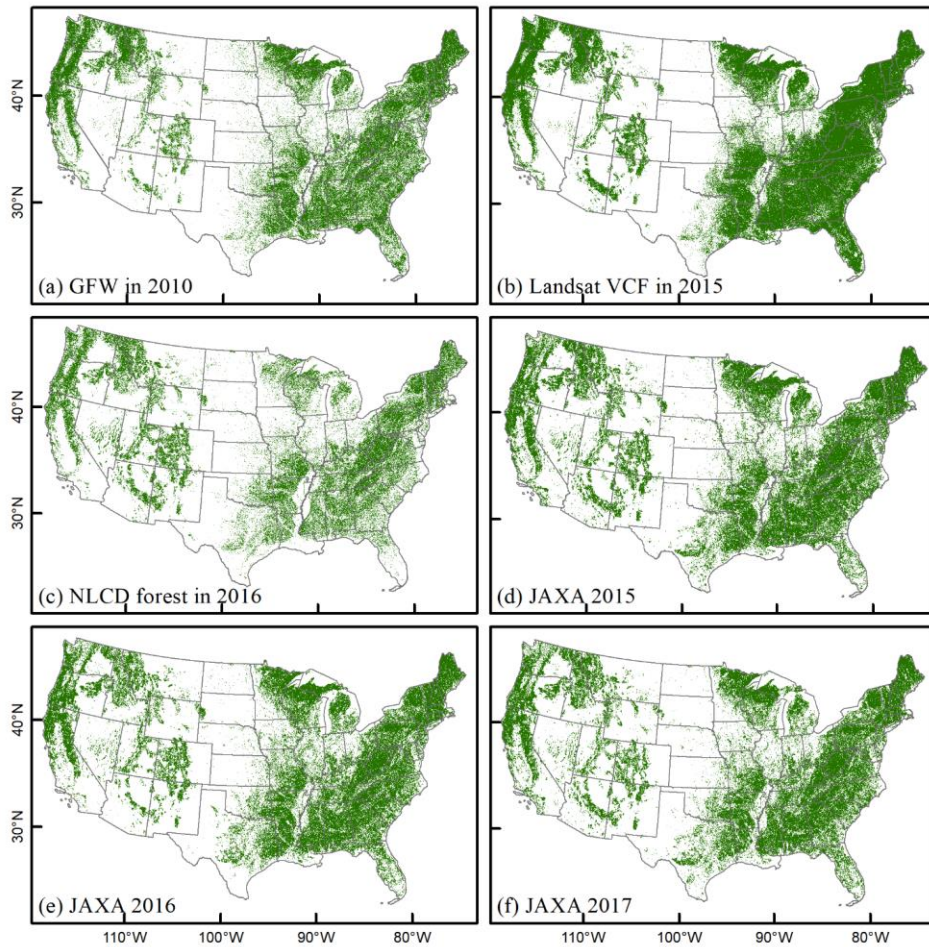
Figure 6: Forest distribution in the CONUS from four forest data products, (a, b, c) Landsat-based and (d, e, f) PALSAR-2-based forest products during 2015-2017.

255   **2.7 PALSAR-2/Landsat forest mapping approach**

The advantages of L-band ALSO-2 PALSAR-2 data in penetrating tree canopy to interact with tree branches and trunks lead to higher volume backscatter signals from forests than from other land cover types (e.g., grasslands, shrublands, croplands, and water bodies). However, some natural surfaces (e.g., rocky lands) or artificial structures (e.g., buildings) also have high backscatter signals, which could easily cause commission errors in the

260   PALSAR/PALSAR-2-based forest signature analysis (Qin et al. 2017). As these land cover types have low NDVI values, they can be tracked and identified by optical images. According to these knowledges, we developed a two-step forest mapping approach by integration of PALSAR or PALSAR-2 and optical (e.g. MODIS, Landsat) images in our previous studies such as in South America (Qin et al. 2017), Asia (Qin et al. 2016b), and Australia (Qin et al. 2021). However, these previous studies were mainly conducted at a lower spatial resolution (e.g., 50-m by PALSAR

265   and MODIS) or attempted for limited spatial scales using PALSAR/PALSAR-2 and Landsat images. It is still unclear that the performance of the integrated datasets for monitoring the annual dynamics of forest distribution and forest functional types over the temperate regions.

In this study, we used the same workflow to identify and map forest cover in CONUS (Qin et al. 2016a). First, we identified forest pixels by using 25-m PALSAR-2 images and the threshold-based algorithm. A pixel is classified

270   to be pixel forest, if its PALSAR-2 data meets $-19 \leq HV \leq -7.5$, $0 \leq Difference \leq 9.5$, $0.2 \leq Ratio \leq 0.95$. The thresholds for the 25-m PALSAR-2 images had been slightly adjusted from those for the 25-m PALSAR data based on our previous studies on PALSAR and PALSAR-2 signature analyses of forest and non-forest samples (Chen et al. 2018; Qin et al. 2016a). A 5×5 window median filter was applied to decrease the potential noise (e.g., salt-and pepper noise) on the PALSAR-based forest and non-forest (F/NF) maps. These resultant 25-m F/NF maps were resampled to 30-m

275   to match the spatial resolution of Landsat images. Forests usually have a high leaf area index (larger than 3 m^2/m^2), but rocky lands, barren lands, and built-up surfaces have no or little green vegetation in a year. Due to LAI and NDVI are closely related to each other, the value of NDVI with 0.7 or so usually represents the range of 1 to 2 m^2/m^2 of LAI dependent upon the vegetation types, which can be used to identify forest and eliminate the commission errors in the PALSAR/PALSAR-2 based forest maps (Qin et al. 2016a). Here we generated the maximum NDVI layers from all

280   the available Landsat images in each year (January to December) during 2015-2017 and applied the threshold of $NDVI_{max} > 0.7$ into the layers to generate the NDVImax masks to extract the pixels covered by green vegetation. The annual 30-m forest map was produced by overlaying the PALSAR-2-based forest maps and the Landsat-based NDVImax mask layers.

In post-classification, a temporal and logical consistency check was performed on this three-year forest and non-

285   forest (F/NF) maps to reduce the noise or misclassification in the F/NF sequence (Chen et al. 2018; Qin et al. 2016a). For each pixel in annual F/NF time series maps from 2015 to 2017, the reasonable forest dynamics were NNN, FNN, NNF, FFF, NFF, and FFN (N denotes non-forest and F indicates forest). The NFN and FNF sequences were considered

as "not reasonable sequence" and re-processed as sequences of NNN and FFF, respectively. This 3-year consistency check during 2015-2017 makes the annual forest map in 2016 with higher confidence, and we will use it for inter-comparison and forest area estimates at county, state, and CONUS scales. The resultant PALSAR-2/Landsat (PL-) annual forest maps are called as "PL-Forest maps" in this study.

2.8 PALSAR-2/Landsat-based annual evergreen forest maps in 2015-2017

Evergreen trees have green leaves all the year round, but deciduous trees usually shed their leaves in winter or dry season. These leaf phenological profiles can be captured by the satellite-based vegetation indices (e.g., NDVI, EVI and LSWI) to distinguish evergreen and deciduous forests (Prabakaran et al. 2013; Qin et al. 2016b). Based on the characteristics of forest canopy phenology and vegetation indices, we have developed a simple and robust algorithms to map evergreen forests by analyzing the time series water-related index (LSWI) and greenness-related indices (EVI, NDVI), and the algorithm has been documented in details in our previous publications (Qin et al. 2016b). We used the same approach and generated annual maps of evergreen vegetation by using the decision thresholds ($FQ_{LSWI \geq 0}$ = 100% and $EVI_{min} \geq 0.2$). Here, the $FQ_{LSWI \geq 0}$ was the observation frequency with LSWI≥0 ($N_{LSWI \geq 0}$) over all the good-quality observations (N_{GOBs}) in a year for individual pixels (EQ. 4), and EVI_{min} was the minimum EVI values in a year. Finally, we overlaid our annual 30-m PALSAR-2/Landsat-based forest/non-forest map with the evergreen vegetation layers to identify evergreen forests.

$$FQ_{LSWI \geq 0} = \frac{N_{LSWI \geq 0}}{N_{GOBs}} \times 100 \qquad (4)$$

2.9 Validation

The resultant PL-Forest maps (forest and non-forest) in 2015-2017 were validated by the validation samples generated by the third party (Fig.4). We overlayed the samples and the resultant PL-Forest maps to calculate the confusion matrix and assess the user's, producer's, and overall accuracies.

2.10 Cross-comparison between forest-related products

We selected five popular forest cover data products at 25-m or 30-m spatial resolution to perform the inter-comparison analysis from two aspects of (1) describing the forest structures and (2) assessing the forest resource areas at different statistic levels.

First, to understand the differences in terms of forest structure measurements in the PALSAR-2-based, Landsat-based, and PALSAR-2/Landsat-based forest maps, we overlaid the ICESat-1 samples and individual forest products to identify those forest pixels that geographically correspond to the ICESat-1 samples and gather their information on the attributes of forest canopy height and canopy coverage. In this process, all the forest products have been resampled into 70-m to match the footprint size of ICESat-1. Then, the distributions of forest pixels were analyzed with the canopy height and canopy coverage for individual forest maps by using 1-D histogram and 2-D histogram graphs.

Secondly, we compared our PL-based forest maps with the selected five forest datasets in terms of forest areas at state and CONUS scales. All the forest maps were re-projected into equal-area projection before the forest areas were calculated from individual maps. The linear regression approach was used to show the relationships in forest areas between these forest datasets at the state level. The forest area estimates at the national level were directly compared among them.

3 Results

3.1 Annual forest and evergreen forest maps in 2015-2017

The PALSAR-2/Landsat forest maps showed the annual forest distribution in CONUS during 2015 to 2017 (Fig.7a, b, c). At the pixel level, we calculated the frequency of individual pixels covered by forest in 2015-2017(Fig.7d). 79% of the forest pixels have consistent forest cover during 2015 to 2017 with a frequency of three, which is much larger than the proportions of forest pixels with one year (11%) or two years (10%) forest cover. The forest dynamics during 2015 to 2017 were shown in Fig.7e, f. It suggested that more forest decrease than forest increase, especially for the central regions.

Based on the third-party validation samples (Fig.4), the accuracies of the PALSAR-2/Landsat forests were high and varied slightly for the years of 2015 to 2017, the overall accuracies of ~93%, the user's accuracies of 87.6% to 95.8%, and producer's accuracies of 90.6% to 91.9% (Table 2). The forest map in 2016 had slightly higher accuracy than 2015 and 2017, which was expected because the temporal and logical consistency check was implemented on the resultant map of 2016 to reduce the noise or misclassification in the F/NF sequence of 2015 to 2017 (see Section 2.7). The accuracies were comparable to the PALSAR-based forest maps that were reported overall accuracies exceeding 91% (Shimada et al. 2014).
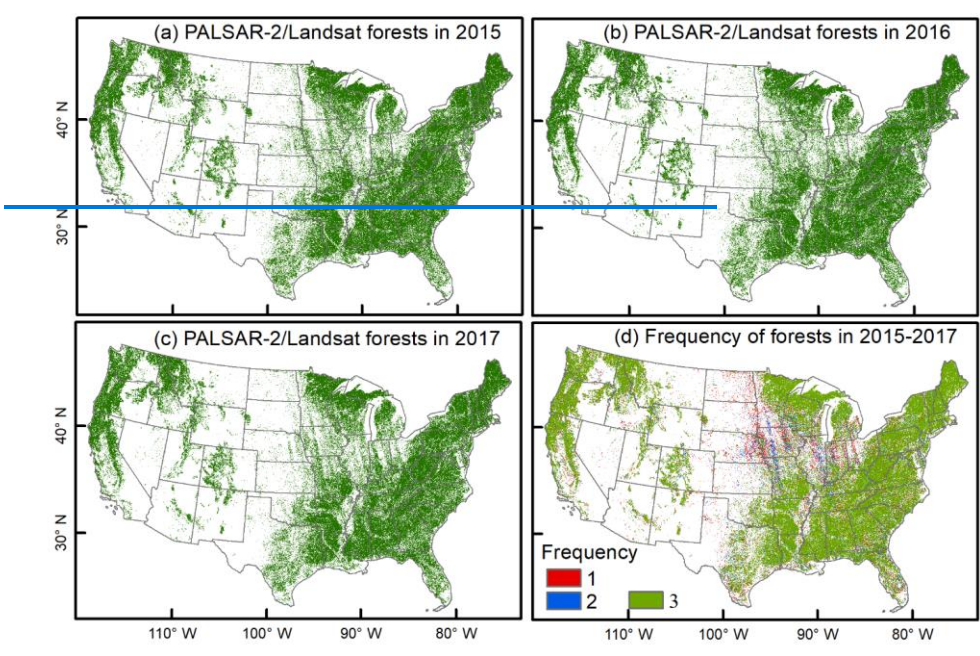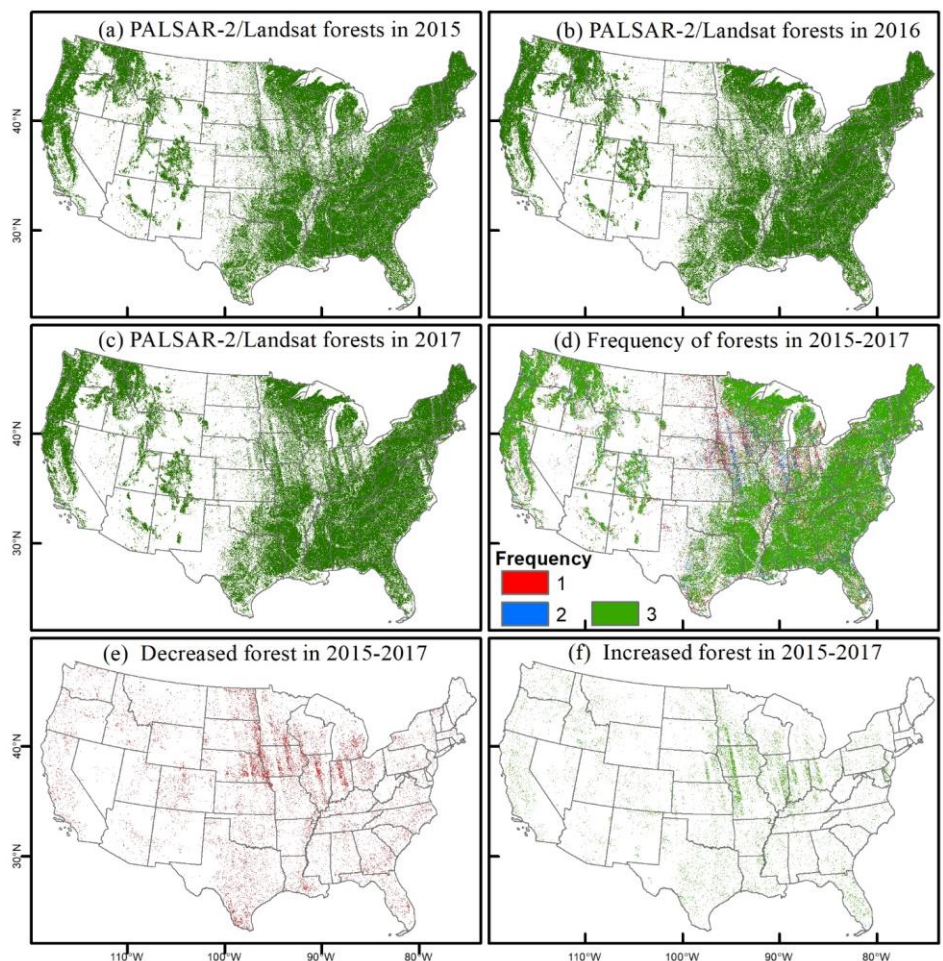
340

Figure 7: Annual forest maps in 2015-2017 based on PALSAR-2 and Landsat images, (a) PL-Forest in 2015, (b) PL-Forest in 2016, and (c) PL-Forest in 2017. (d) the forest frequency map generated based on the PL-Forest maps in 2015-2017. (e) the decreased forest in 2015-2017. (f) the increased forest in 2015-2017.

345   Table 2. Accuracy assessment of annual PALSAR-2/Landsat forest maps in 2015-2017 (PL-Forests) based on the third-party validation samples (Fig.4). The User's (UA), Producer's (PA) and Overall (OA) accuracy are shown.

PL-Forests Classification		Reference			UA	PA	OA
		Forests	Non-Forests	Total			
2015	Forests	596	84	680	87.6%	91.4%	92.8%
	Nonforests	56	1222	1278	95.6%	93.5%	

	Total	652	1306	1958			
2016	Forests	599	81	680	88.1%	91.9%	93.2%
	Nonforests	53	1225	1278	95.8%	93.8%	
	Total	652	1306	1958			
2017	Forests	591	84	675	87.6%	90.6%	92.6%
	Nonforests	61	1222	1283	95.2%	93.5%	
	Total	652	1306	1958			

Based on the PALSAR-2/Landsat forest maps, we further identified annual evergreen forests in CONUS during 2015-2017 (Fig. 8a, b, c). These resultant evergreen forest maps have similar spatial patterns with the evergreen forests in the NLCD-2016 dataset (Fig. 8d). Evergreen forests show obvious regional characteristics and are mainly distributed in the western, southeastern, and northeastern regions of the CONUS. The evergreen forest area estimated from the PALSAR-2/Landsat map in 2016 was 1.08×10^6 km^2, which is higher than the evergreen forests of 0.92×10^6 km^2 but lower than the total area of evergreen forests and mixed forests of 1.22×10^6 km^2 from the NLCD-2016 (Fig. 8a-d). The spatial comparison between these two products was carried out at the pixel scale (Fig. 8e). The noticeable discrepancies were in the southwestern regions (e.g., Nevada, Utah, Arizona), the south Florida, and some regions in the northeastern CONUS. In the southwestern regions, the differences were mainly from the detection of evergreen and non-evergreen forests between these two products. For the eastern regions (e.g., south Florida, New England states), the differences of these two products were mostly caused by the detection of forests, as most of the evergreen forest pixels in the PALSAR-2/Landsat evergreen forest map were shown as non-forest in the NLCD map (Fig. 8e). At the state scale, the PALSAR-2/Landsat evergreen forest map in 2016 had a good linear relationship with the evergreen forests in NLCD 2016, with a slope of 0.8 and R^2 of 0.54 (Fig. 8f). A stronger relationship was found between the evergreen forest areas from the PL-Evergreen forest maps and the sum of evergreen forest and mixed forests from the NLCD-2016 at the state scale, with a slope of 0.98 and R^2 of 0.69 (Fig. 8f). One possible explanation could be that the mixed forests in NLCD include evergreen species (Selkowitz and Stehman 2011). However, it cannot be estimated quantitatively because it is uncertain about the forest types and proportions within the mixed forest pixels (Tran et al. 2016).
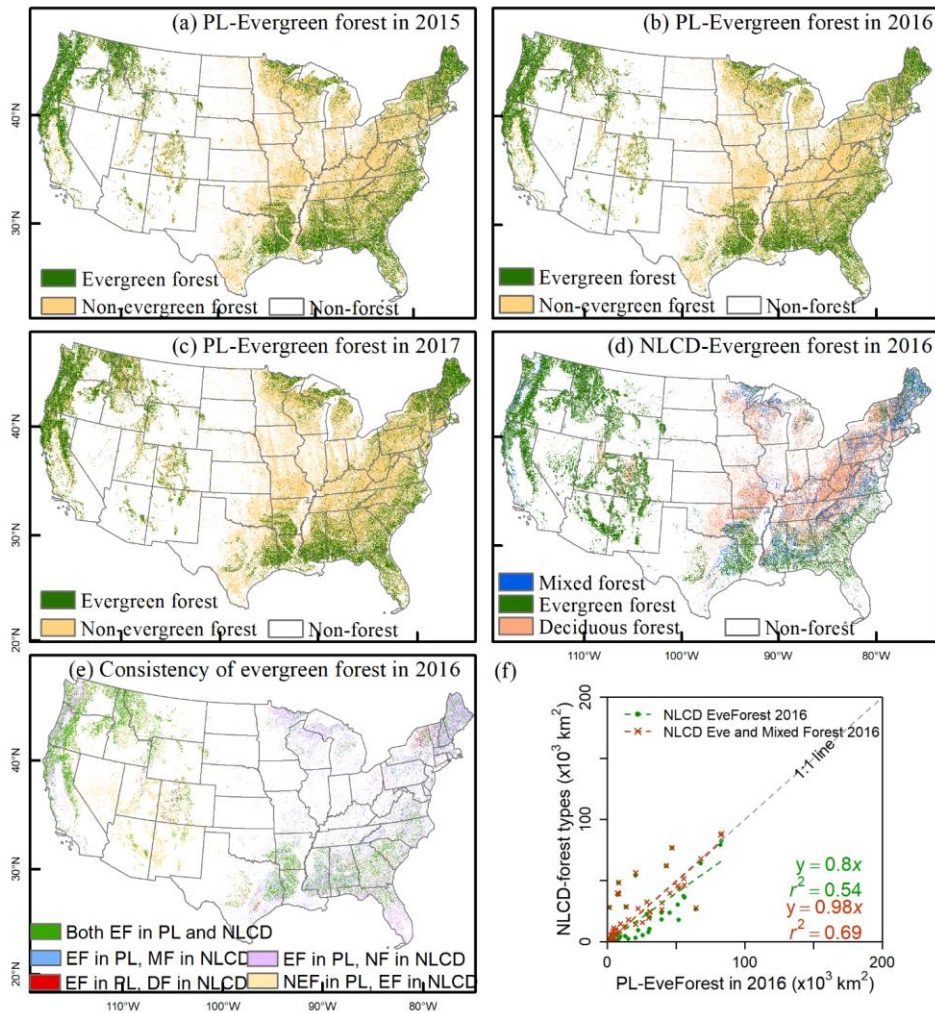
Figure 8: Spatial distributions of evergreen forests in the CONUS. (a, b, c) Annual evergreen and non-evergreen forest maps in 2015-2017. (d) The forest type map from the NLCD 2016 dataset. (d) shows the consistency between the PALSAR-2/Landsat evergreen forest (PL-Evergreen) in 2016 and the NLCD evergreen forest in 2016 (NLCD-Evergreen). (f) shows the comparison between PL- and NLCD-Evergreen forests at the state scale using the linear regression analysis.

3.2 A comparison of five satellite-based forest maps at the pixel scale

At the pixel scale, we compared the PALSAR-2/Landsat forests and the JAXA forests in 2016 in terms of forest

area identification (Fig. 9). These two products have about 75% pixels in agreement, 11% pixels only identified in the

375 JAXA forests, and 14% pixels only in the PALSAR-2/Landsat forest product. Comparison through zoom-in random

samples showed that JAXA forests identified the pixels with obvious background of barren lands or rocks, which were

excluded in the PALSAR-2/Landsat forests. However, JAXA forests missed more pixels with dense tree cover, which

were identified in the PALSAR-2/Landsat forests (Fig.9).

We further compared the five studied satellite-based forest data products in terms of their forest definitions of

380 canopy (tree) height (CH) and canopy coverage (CC). The frequency distributions of the forest pixels with CH and

CC were extracted from different forest products using ICESat-1 observations (Fig. 10). The comparison result

showed that the proportion of forest pixels with CH larger than 5-m and CC larger than 10% was 85% for NLCD-

2016, ~82% for PALSAR-2/Landsat, 81% for JAXA, 80% for GFW 2010 (79.98%), and 77% for Landsat VCF 2015.
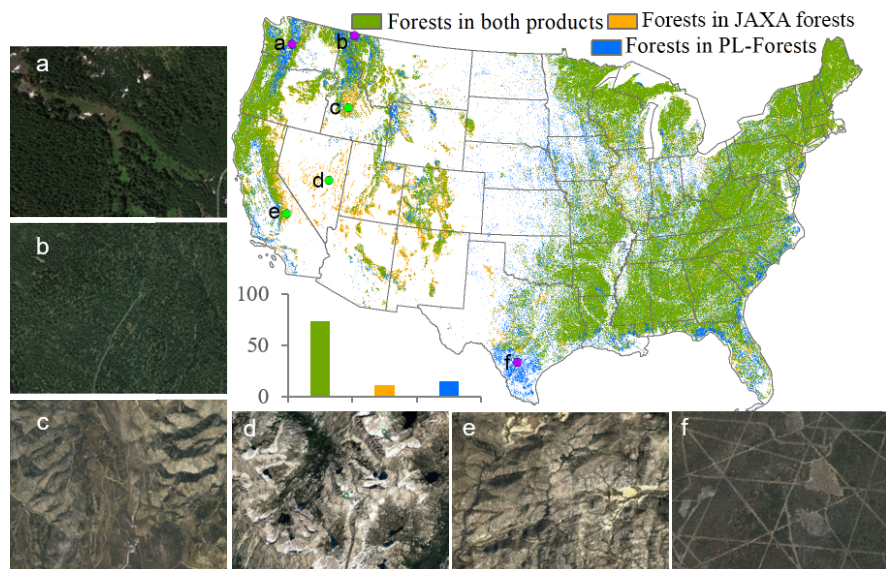
385 **Figure 9: A comparison between PL-forest in 2016 and JAXA forest in 2016 at the pixel scale. Six random areas denoted as a to f were selected from the disagreement regions, which were used to show the zoom-in landscapes from the Google Earth high resolution images. The images were acquired from Google Earth Pro (© Google Earth Pro 2020)**
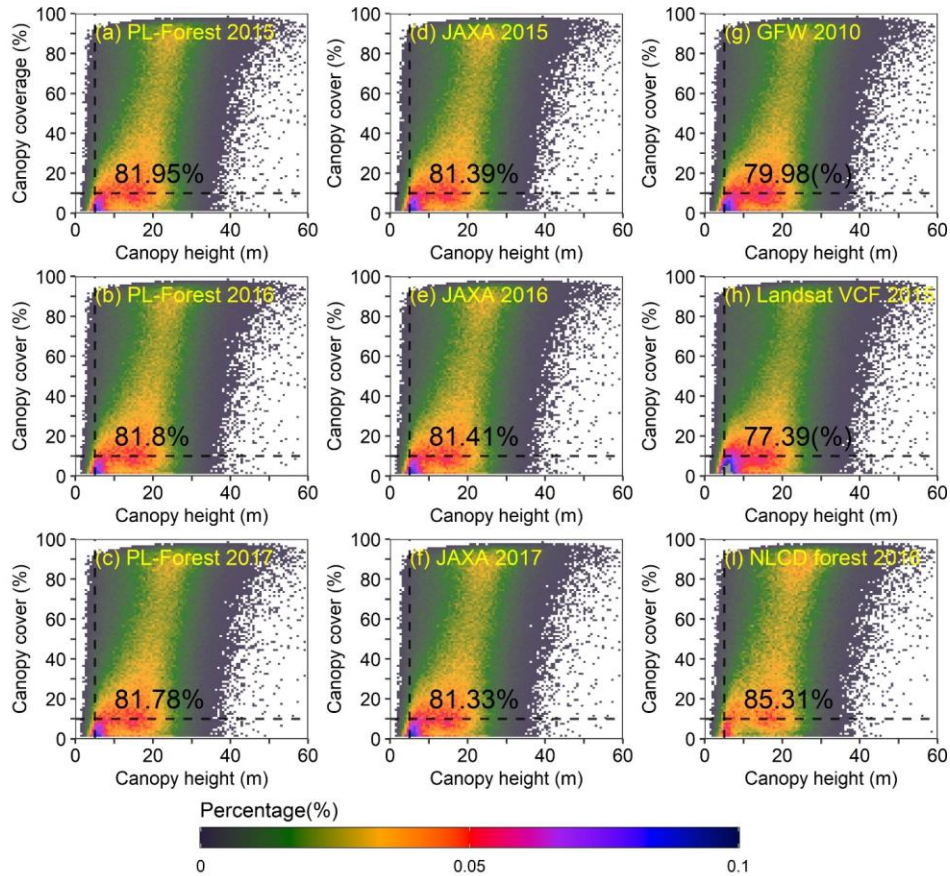
Figure 10: The frequency distributions of the forest pixels with tree canopy height (CH) and canopy cover (CC) features. The forest pixels were from the five satellite-based forest products, respectively. The CH and CC data were extracted from the ICESat-1 observations.

3.3 A comparison of forest area estimates from six forest datasets at state and CONUS scales

The forest areas were estimated at the state and the CONUS scales from the six forest datasets, including five satellite-based forest maps in 2010-2017 and a FIA statistic data in 2017 (Fig. 11). At the state scale, the PALSAR-2/Landsat forest maps have good linear relationships with other satellite-based datasets for each year during 2015 to 2017, with the slope ranging from 0.65 to 1.15, R^2 within 0.87 to 0.96 (Fig. 11a, b, c). In terms of forest area estimates at the state scale, the PL- and JAXA forest maps showed higher agreements with the FIA forest dataset than do GFW 2010, Landsat VCF 2015, and NLCD 2016 forest maps (Fig. 11d). The forest area estimates from the Landsat VCF

in 2015 was higher than the FIA forest area estimates (slope of 1.19), while the forest area estimates from the GFW 2010 and NLCD 2016 were lower than the FIA forest area estimates (slopes of 0.89 and 0.71) (Fig. 11d). The forest area estimates from the PL-Forest and JAXA forest maps were very close to the numbers from the FIA (a slope of 0.98).

At the CONUS scale, the forest area estimates from the PALSAR-2/Landsat forest maps for years of 2015 to 2017 were 2.73×10^6 km^2, 2.79×10^6 km^2 and 2.66×10^6 km^2, respectively, which were similar to the areas of JAXA forests of 2.79×10^6 km^2, 2.68×10^6 km^2 and 2.62×10^6 km^2 (Fig. 11e). The FIA dataset reported the forest area of 2.57×10^6 km^2 in 2017, which was very close to the value of 2.66×10^6 km^2 from the PL-Forest map in 2017, a difference of 3.5%.
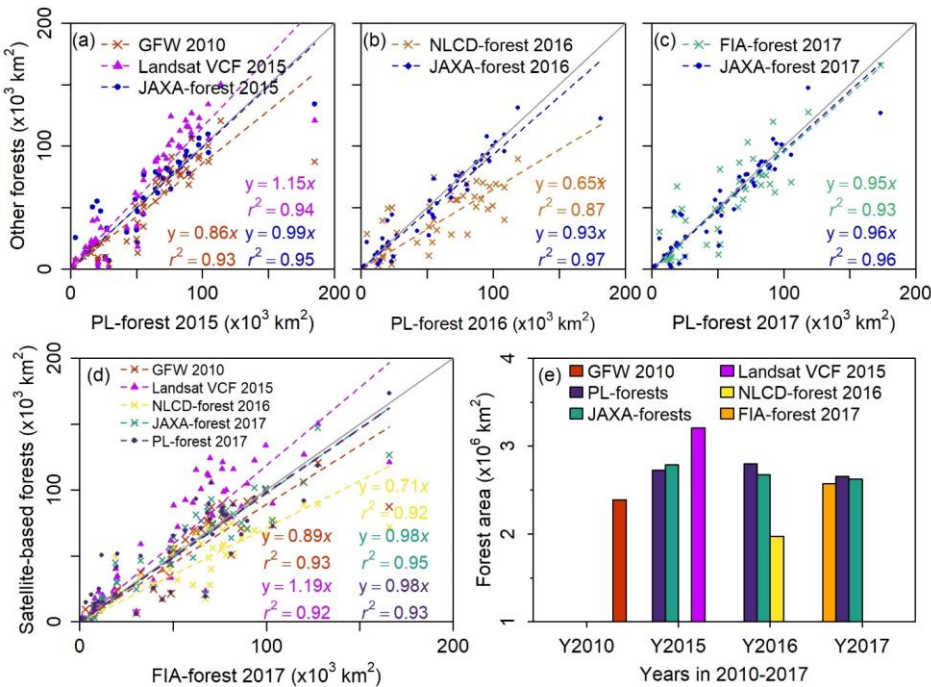
Figure 11: The comparisons of forest area estimates between satellite-based forest products and the FIA statistics at the state and national scales.

4 Discussion

4.1 Improved annual forest maps at high spatial resolution

  To improve the accuracy of forest cover maps, several efforts have examined the likely factors causing the uncertainties of the resultant products (Qin et al. 2016b; Sexton et al. 2016; Sexton et al. 2013a; Tchuenté et al. 2011).

415 These factors include (1) the diverse forest-cover definitions, (2) input image datasets, (3) training samples, and (4) algorithms (Qin et al. 2021; Tchuenté et al. 2011). For example, the forest definitions use different criteria of tree coverage (from 10% to 60%) and tree height (from 2-m to 5-m), as well as the parcel size (Qin et al. 2016b; Sexton et al. 2016). To reduce the uncertainty of forest maps in the perspective of forest definition, a solution was proposed by Sexton et al. (2016) to focus on the measurable ecological characteristics of tree cover, canopy height, biomass,

420 and composition of vegetation. According to the FAO forest definition and the Lidar-based comparison between forest datasets, the PL-Forest had slightly higher percentage of pixels than JAXA-Forest, GFW 2010, and Landsat VCF 2015 in the criteria of tree height larger than 5-m and/or canopy cover larger than 10%. In this criterion, the NLCD forest 2016 had the highest pixel proportion, but this dataset used the tree canopy cover larger than 20% as the forest threshold and resulted in the lowest forest area estimate (Fig. 11e). This comparison results based on the PALSAR-

425 2/Landsat forests agree well with our recent study on the forest mapping in Australia, which demonstrated that PALSAR/MODIS forest maps had more forest pixels satisfied with the FAO's forest definition than the GFW and JAXA forest maps (Qin et al. 2021).

  Forest area data products have been generated based on the optical images (e.g., MODIS, Landsat), microwave images (e.g. PALSAR, PALSAR-2), or the integration of microwave and optical images (e.g. PALSAR/MODIS,

430 PALSAR/Landsat). On the forest area estimates, under a consistent tree canopy cover definition (10%), the PALSAR-2/Landsat products had close results to the PALSAR-2-based forest maps for years of 2015 to 2017 at both state and national scales (Fig. 11). The forest area estimates in 2017 from the PL-Forest dataset was very close to the result from the FIA dataset, which indicates that the PL-Forest dataset is more accurate than the forest area estimates from the other optical satellite-based forest products (Fig. 11e). Our previous studies also showed the similar forest area

435 estimates from the PALSAR/MODIS or PALSAR/Landsat forest products and the JAXA forest maps in several regions like monsoon Asia (Qin et al. 2016b), and South America (Qin et al. 2017). For example, in the South America, forest area estimates from the 30-m GFW-2010 dataset were higher than those from the 50-m PALSAR/MODIS forest products (Qin et al. 2017).

The results mentioned above also suggested that PL-Forests had a slightly better performance than the other four forest products, according to the potential of forest tree height and tree canopy cover monitoring, and forest area estimates. This result corroborates the previous claims for integrating microwave and optical images to improve the forest cover maps (Lehmann et al. 2015; Reiche et al. 2015; Thapa et al. 2014). These forest mapping approaches take advantage of (1) the sensitivity of microwave signals to forest structures without weather interference (Næsset et al. 2016; Qin et al. 2016b), and (2) the optical signals to reduce the ground objects with similar backscatter values as forests, such as rocky lands and buildings (Lehmann et al. 2015; Reiche et al. 2015) (Fig.9). The integration of PALSAR and MODIS images has been demonstrated to generate improved forest maps in tropical, temperate, and boreal forests with overall accuracies above 90% (Qin et al. 2016b; Qin et al. 2017; Zhang et al. 2019). This study produced the forest maps with overall accuracy about 93% that corroborated the potential of combining suggested that the approach based on PALSAR-2 and Landsat observations has the potential to monitor the annual dynamics of forest distribution and functional types at a high spatial resolution for national or larger scales across the temperate regions.

However, there could be some uncertainties and limitations when applying this approach. Firstly, although the thresholds of PALSAR-2 signatures for extracting forests were trained by numerous samples, they could be impacted by forest composition and structures (Chen et al. 2018). Thus, a careful study of the thresholds by samples of specific areas could provide more information that affect the accuracy and uncertainty of the forest maps when applying the algorithms into other regions. In addition, due to the PALSAR data are not available during 2011-2014, we cannot apply this PALSAR/optical data approach in these four years. PALSAR data are available for 2007-2010, thus a combination of PALSAR (2007-2010), PALSAR-2 (2015 to present), and optical images would develop forest maps to monitor forest changes since 2007 (Zhang et al. 2019).

4.2 Evergreen forest mapping algorithms

Evergreen forests show different functional traits from deciduous forests, such as water use efficiency (Soh et al. 2019), high ecosystem stability in carbon sink under extreme climates (Huang and Xia 2019). Driven by climate change and diverse human activities, the expansion of evergreen forests has been reported in many regions over the word (Saintilan and Rogers 2015; Twidwell et al. 2016). Various mapping algorithms have been developed to identify evergreen and non-evergreen forests, which could provide the accurate information on evergreen forests for science and policy users (Qin et al. 2016b). These evergreen forest mapping algorithms can be grouped as (1) NDVI-based

and (2) LSWI-based algorithms. Evergreen plants keep green leaves in winter season or dry season and yield high NDVI values in contrast to senescent plants. Following this phenological feature, evergreen plants and forests have been successfully separated from non-evergreen plants based on the seasonal dynamics of NDVI, for example using

470   mean or median NDVI values of winter season (Qin et al. 2016b; Soudani et al. 2012). Evergreen forests have LSWI values of above zero throughout the year, which has been used to map evergreen forest for tropical regions (Grogan et al. 2016; Qin et al. 2016b). In this study, the LSWI-based algorithm was used to identify the evergreen forests in CONUS and the results have reasonable consistency with the NLCD-2016 evergreen forest product (Fig. 8). It demonstrated the potential of the LSWI-based algorithm for the evergreen forest identification over the temperate

475   regions based on Landsat datasets.

The moderate discrepancy of the evergreen forest products between the PL-Forest maps and the NLCD-2016 dataset could be attributed in part to the differences in the algorithms and image data. The NLCD products were generated using the decision tree algorithm and multi-temporal images (Jin et al. 2019). The classification algorithm is based on the spatial statistics of images (image-based spatial statistics) and training samples to generate

480   classification rule. Therefore, the resultant forest maps are affected by the quantity and quality of the training samples. In comparison, we used the LSWI-based algorithm and time series images in a year to identify forests for individual pixels, which used the pixel-based time series statistics. Our method used all the images in a year, which is more than multi-temporal images used in the image-based spatial statistic approach. A challenge for the LSWI-base algorithm is to acquire sufficient number of good quality observations throughout the year, in particular, during the winter season.

485   As Landsat acquires images at 16-day revisit cycle, the missing data issue could cause some uncertainties in the PALSAR-2/Landsat evergreen forest maps. However, this data issue could be improved by combining multi-source remote sensing images like Sentinle-2, Landsat-8 and Landsat-9 in the future. To improve the evergreen forest mapping, development of a hybrid approach of both LSWI- and NDVI-based algorithms is another promising way, which will be examined in our following works for discrimination of evergreen and deciduous trees, shrubs, and

490   grasses.

Data availability

The data are available at https://doi.org/10.6084/m9.figshare.21270261 (Wang et al., 2022).

Conclusions

This study integrated microwave (PALSAR-2) and optical (Landsat) images and produced annual ~~30 m~~ forest maps in 2015-2017 for the CONUS at 30-m spatial resolution. We compared the PL-based forest maps with the four widely-used satellite-based forest maps in terms of (1) forest area estimates and (2) forest definition by forest structure metrics (tree height and canopy coverage) from the ICESat LiDAR tree structure datasets. The good performance of PL-based forest maps shows the strong potential of the PALSAR-2/Landsat integrated mapping approach for generating accurate high-resolution forest products at the national or larger scales. Furthermore, we generated the annual 30-m evergreen forest maps in the CONUS, which can be used to investigate how climate change and human activities affect these forest types in the CONUS. The investigation on the satellite-based forest mapping approaches and the FIA forest products also suggested the potential of integrating FIA data and PALSAR and Landsat images to support the FAO's Global Forest Resources Assessment at the national scale.

Competing interests

The authors declare that they have no known competing financial interests or personal relationships that could have appeared to influence the work reported in this paper.

Author contribution

Xiangming Xiao and Jie Wang designed the experiments and Jie Wang carried them out. Jie Wang, Yuanwei Qin, Jinwei Dong developed the model code. Jie Wang prepared the manuscript with contributions from all co-authors.

Acknowledgements

The authors greatly appreciated the free access to the PALSAR-2, Landsat datasets provided by USGS and Google Earth Engine cloud computing platform, the public forest datasets of GFW in 2010 from the GLAD, the Landsat VCF in 2015 from the LCLUC, JAXA forest and non-forest maps in 2015-2017, the NLCD land cover map in 2016 from USGS, the forest statistical data for year 2017 from the USDA, and the free access to the validation samples provided by the Tsinghua University. We also thank the editor and reviewers for the insightful comments and suggestions.

Financial support

This study is funded by the National Natural Science Foundation of China (42101355), the Key Research and
520   Development Program of Ningxia Province, China (2022BEG03050), the National Science Foundation (IIA-1920946, IIA-1946093), and USDA National Institute of Food and Agriculture (2016-68002-24967).

References

Achard, F., Eva, H., & Mayaux, P. (2001). Tropical forest mapping from coarse spatial resolution satellite data: production and accuracy assessment issues. *International Journal of Remote Sensing,*
525   *22*, 2741-2762

Betts, M.G., Wolf, C., Ripple, W.J., Phalan, B., Millers, K.A., Duarte, A., Butchart, S.H., & Levi, T. (2017). Global forest loss disproportionately erodes biodiversity in intact landscapes. *Nature, 547*, 441-444

Bonan, G.B. (2008). Forests and climate change: Forcings, feedbacks, and the climate benefits of
530   forests. *Science, 320*, 1444-1449

Burrill, E.A., DiTommaso, A.M., Turner, J.A., Pugh, S.A., Menlove, J., Christiansen, G., Perry, C.J., & Conkling, B.L. (2021). The Forest Inventory and Analysis Database: database description and user guide version 9.0.1 for Phase 2. In (p. 1026 p): U.S. Department of Agriculture, Forest Service

535   Chen, B.Q., Xiao, X.M., Ye, H.C., Ma, J., Doughty, R., Li, X.P., Zhao, B., Wu, Z.X., Sun, R., Dong, J.W., Qin, Y.W., & Xie, G.S. (2018). Mapping Forest and Their Spatial-Temporal Changes From 2007 to 2015 in Tropical Hainan Island by Integrating ALOS/ALOS-2 L-Band SAR and Landsat Optical Images. *Ieee Journal of Selected Topics in Applied Earth Observations and Remote Sensing, 11*, 852-867

540   Chen, J., Chen, J., Liao, A., Cao, X., Chen, L., Chen, X., He, C., Han, G., Peng, S., & Lu, M. (2015). Global land cover mapping at 30 m resolution: A POK-based operational approach. *Isprs Journal of Photogrammetry and Remote Sensing, 103*, 7-27

D'Almeida, C., Vörösmarty, C.J., Hurtt, G.C., Marengo, J.A., Dingman, S.L., & Keim, B.D. (2007). The effects of deforestation on the hydrological cycle in Amazonia: a review on scale and
545   resolution. *International Journal of Climatology: A Journal of the Royal Meteorological Society, 27*, 633-647

Deb Burman, P.K., Launiainen, S., Mukherjee, S., Chakraborty, S., Gogoi, N., Murkute, C., Lohani, P., Sarma, D., & Kumar, K. (2021). Ecosystem-atmosphere carbon and water exchanges of subtropical evergreen and deciduous forests in India. *Forest Ecology and Management, 495*,
550   119371

DiMiceli, C., Carroll, M., Sohlberg, R., Huang, C., Hansen, M., & Townshend, J. (2017). Annual global automated MODIS vegetation continuous fields (MOD44B) at 250 m spatial resolution for data years beginning day 65, 2000? 2010, collection 5 percent tree cover. *University of Maryland, College Park, MD, USA*

555   Domke, G.M., Walters, B.F., Nowak, D.J., Smith, J., Nichols, M.C., Ogle, S.M., Coulston, J., & Wirth, T.J.R.U.F.M., WI: US Department of Agriculture, Forest Service, Northern Research Station. 5 p.. (2021). Greenhouse gas emissions and removals from forest land, woodlands, and urban trees in the United States, 1990–2019*, 307*

FAO (2012). Forest Resources Assessments (FRA2010). In. Rome: Food and Agricultural Organization of the United Nations.

Foley, J.A., DeFries, R., Asner, G.P., Barford, C., Bonan, G., Carpenter, S.R., Chapin, F.S., Coe, M.T., Daily, G.C., Gibbs, H.K., Helkowski, J.H., Holloway, T., Howard, E.A., Kucharik, C.J., Monfreda, C., Patz, J.A., Prentice, I.C., Ramankutty, N., & Snyder, P.K. (2005). Global consequences of land use. *Science, 309*, 570-574

Friedl, M.A., Sulla-Menashe, D., Tan, B., Schneider, A., Ramankutty, N., Sibley, A., & Huang, X.M. (2010). MODIS Collection 5 global land cover: Algorithm refinements and characterization of new datasets. *Remote Sensing of Environment, 114*, 168-182

Gong, P., Wang, J., Yu, L., Zhao, Y.C., Zhao, Y.Y., Liang, L., Niu, Z.G., Huang, X.M., Fu, H.H., Liu, S., Li, C.C., Li, X.Y., Fu, W., Liu, C.X., Xu, Y., Wang, X.Y., Cheng, Q., Hu, L.Y., Yao, W.B., Zhang, H., Zhu, P., Zhao, Z.Y., Zhang, H.Y., Zheng, Y.M., Ji, L.Y., Zhang, Y.W., Chen, H., Yan, A., Guo, J.H., Yu, L., Wang, L., Liu, X.J., Shi, T.T., Zhu, M.H., Chen, Y.L., Yang, G.W., Tang, P., Xu, B., Giri, C., Clinton, N., Zhu, Z.L., Chen, J., & Chen, J. (2013). Finer resolution observation and monitoring of global land cover: first mapping results with Landsat TM and ETM+ data. *International Journal of Remote Sensing, 34*, 2607-2654

Grogan, K., Pflugmacher, D., Hostert, P., Verbesselt, J., & Fensholt, R. (2016). Mapping Clearances in Tropical Dry Forests Using Breakpoints, Trend, and Seasonal Components from MODIS Time Series: Does Forest Type Matter? *Remote Sensing, 8*

Hansen, M., Potapov, P., Moore, R., Hancher, M., Turubanova, S., Tyukavina, A., Thau, D., Stehman, S., Goetz, S., & Loveland, T. (2013a). High-resolution global maps of 21st-century forest cover change. *Science, 342*, 850-853

Hansen, M.C., & DeFries, R.S. (2004). Detecting long-term global forest change using continuous fields of tree-cover maps from 8-km advanced very high resolution radiometer (AVHRR) data for the years 1982-99. *Ecosystems, 7*, 695-716

Hansen, M.C., DeFries, R.S., Townshend, J.R.G., Carroll, M., Dimiceli, C., & Sohlberg, R.A. (2003). Global Percent Tree Cover at a Spatial Resolution of 500 Meters: First Results of the MODIS Vegetation Continuous Fields Algorithm. *Earth Interactions, 7*

Hansen, M.C., Potapov, P.V., Moore, R., Hancher, M., Turubanova, S., Tyukavina, A., Thau, D., Stehman, S., Goetz, S., & Loveland, T. (2013b). High-resolution global maps of 21st-century forest cover change. *Science, 342*, 850-853

Harris, N.L., Brown, S., Hagen, S.C., Saatchi, S.S., Petrova, S., Salas, W., Hansen, M.C., Potapov, P.V., & Lotsch, A. (2012). Baseline map of carbon emissions from deforestation in tropical regions. *Science, 336*, 1573-1576

Homer, C., Dewitz, J., Jin, S., Xian, G., Costello, C., Danielson, P., Gass, L., Funk, M., Wickham, J., Stehman, S., Auch, R., & Riitters, K. (2020). Conterminous United States land cover change patterns 2001–2016 from the 2016 National Land Cover Database. *Isprs Journal of Photogrammetry and Remote Sensing, 162*, 184-199

Hoover, C.M., Bush, R., Palmer, M., & Treasure, E. (2020). Using Forest Inventory and Analysis Data to Support National Forest Management: Regional Case Studies. *Journal of Forestry, 118*, 313-323

Huang, K., & Xia, J. (2019). High ecosystem stability of evergreen broadleaf forests under severe droughts. *Global change biology, 25*, 3494-3503

Jin, S., Homer, C., Yang, L., Danielson, P., Dewitz, J., Li, C., Zhu, Z., Xian, G., & Howard, D. (2019). Overall Methodology Design for the United States National Land Cover Database 2016 Products. *Remote Sensing, 11*, 2971

605 Jin, S., Yang, L., Danielson, P., Homer, C., Fry, J., & Xian, G. (2013a). A comprehensive change detection method for updating the National Land Cover Database to circa 2011. *Remote Sensing of Environment, 132*, 159-175

Jin, S.M., Yang, L.M., Danielson, P., Homer, C., Fry, J., & Xian, G. (2013b). A comprehensive change detection method for updating the National Land Cover Database to circa 2011. *Remote*
610 *Sensing of Environment, 132*, 159-175

Knott, J.A., Desprez, J.M., Oswalt, C.M., & Fei, S.L. (2019). Shifts in forest composition in the eastern United States. *Forest Ecology and Management, 433*, 176-183

Kushwaha, S.P.S. (1990). Forest-Type Mapping and Change Detection from Satellite Imagery. *Isprs Journal of Photogrammetry and Remote Sensing, 45*, 175-181

615 Laurin, G.V., Puletti, N., Hawthorne, W., Liesenberg, V., Corona, P., Papale, D., Chen, Q., & Valentini, R. (2016). Discrimination of tropical forest types, dominant species, and mapping of functional guilds by hyperspectral and simulated multispectral Sentinel-2 data. *Remote Sensing of Environment, 176*, 163-176

Lehmann, E.A., Caccetta, P., Lowell, K., Mitchell, A., Zhou, Z.-S., Held, A., Milne, T., & Tapley,
620 I. (2015). SAR and optical remote sensing: Assessment of complementarity and interoperability in the context of a large-scale operational forest monitoring system. *Remote Sensing of Environment, 156*, 335-348

Mekonnen, Z.A., Riley, W.J., Randerson, J.T., Grant, R.F., & Rogers, B.M. (2019). Expansion of high-latitude deciduous forests driven by interactions between climate warming and fire. *Nature*
625 *Plants, 5*, 952-958

Næsset, E., Ørka, H.O., Solberg, S., Bollandsås, O.M., Hansen, E.H., Mauya, E., Zahabu, E., Malimbwi, R., Chamuya, N., Olsson, H., & Gobakken, T. (2016). Mapping and estimating forest area and aboveground biomass in miombo woodlands in Tanzania using data from airborne laser scanning, TanDEM-X, RapidEye, and global forest maps: A comparison of estimated precision.
630 *Remote Sensing of Environment, 175*, 282-300

Oswalt;, S.N., Smith;, W.B., Miles;, P.D., & Pugh, S.A. (2019). Assessment of the influence of disturbance, management activities, and environmental factors on carbon stocks of U.S. national forests. In, *General Technical Report (GTR)*. Gen. Tech. Rep. WO-97. Washington, DC: U.S. Department of Agriculture, Forest Service, Washington Office.

635 Peng, S.S., Piao, S.L., Zeng, Z.Z., Ciais, P., Zhou, L.M., Li, L.Z.X., Myneni, R.B., Yin, Y., & Zeng, H. (2014). Afforestation in China cools local land surface temperature. *Proceedings of the National Academy of Sciences of the United States of America, 111*, 2915-2919

Prabakaran, C., Singh, C., Panigrahy, S., & Parihar, J.J.C.S. (2013). Retrieval of forest phenological parameters from remote sensing-based NDVI time-series data, 795-802

640 Qin, Y., Xiao, X., Wang, J., Dong, J., Ewing, K., Hoagland, B., Hough, D., Fagin, T., Zou, Z., Geissler, G., Xian, G., & Loveland, T. (2016a). Mapping Annual Forest Cover in Sub-Humid and Semi-Arid Regions through Analysis of Landsat and PALSAR Imagery. *Remote Sensing, 8*, 933

Qin, Y., Xiao, X., Wigneron, J.-P., Ciais, P., Canadell, J.G., Brandt, M., Li, X., Fan, L., Wu, X., & Tang, H. (2021). Annual Maps of Forests in Australia from Analyses of Microwave and Optical
645 Images with FAO Forest Definition. *Journal of remote sensing, 2021*

Qin, Y.W., Xiao X.M., Dong, J.W., Zhang, G.L., Roy, P.S., Joshi, P.K., Gilani, H., Murthy, M.S.R., Jin, C., Wang, J., Zhang, Y., Chen, B.Q., Menarguez, M.A., Biradar, C.M., Bajgain, R., Li, X.P., Dai, S.Q., Hou, Y., Xin, F.F., & Moore, B. (2016b). Mapping forests in monsoon Asia with ALOS PALSAR 50-m mosaic images and MODIS imagery in 2010. *Scientific Reports, 6*

650   Qin, Y.W., Xiao, X.M., Dong, J.W., Zhang, Y., Wu, X.C., Shimabukuro, Y., Arai, E., Biradar, C., Wang, J., Zou, Z.H., Liu, F., Shi, Z., Doughty, R., & Moore, B. (2019). Improved estimates of forest cover and loss in the Brazilian Amazon in 2000-2017. *Nature Sustainability, 2*, 764-772

Qin, Y.W., Xiao, X.M., Dong, J.W., Zhou, Y.T., Wang, J., Doughty, R.B., Chen, Y., Zou, Z.H., & Moore, B. (2017). Annual dynamics of forest areas in South America during 2007-2010 at 50m

655   spatial resolution. *Remote Sensing of Environment, 201*, 73-87

Reiche, J., Hamunyela, E., Verbesselt, J., Hoekman, D., & Herold, M. (2018). Improving near-real time deforestation monitoring in tropical dry forests by combining dense Sentinel-1 time series with Landsat and ALOS-2 PALSAR-2. *Remote Sensing of Environment, 204*, 147-161

Reiche, J., Verbesselt, J., Hoekman, D., & Herold, M. (2015). Fusing Landsat and SAR time series

660   to detect deforestation in the tropics. *Remote Sensing of Environment, 156*, 276-293

Saintilan, N., & Rogers, K. (2015). Woody plant encroachment of grasslands: a comparison of terrestrial and wetland settings. *New Phytologist, 205*, 1062-1070

Selkowitz, D.J., & Stehman, S.V. (2011). Thematic accuracy of the National Land Cover Database (NLCD) 2001 land cover for Alaska. *Remote Sensing of Environment, 115*, 1401-1407

665   Seto, K.C., Guneralp, B., & Hutyra, L.R. (2012). Global forecasts of urban expansion to 2030 and direct impacts on biodiversity and carbon pools. *Proceedings of the National Academy of Sciences of the United States of America, 109*, 16083-16088

Sexton, J.O., Noojipady, P., Song, X.-P., Feng, M., Song, D.-X., Kim, D.-H., Anand, A., Huang, C., Channan, S., & Pimm, S.L. (2016). Conservation policy and the measurement of forests.

670   *Nature Climate Change, 6*, 192-196

Sexton, J.O., Noojipady, P., Song, X.-P., Feng, M., Song, D.-X., Kim, D.-H., Anand, A., Huang, C., Channan, S., Pimm, S.L., & Townshend, J.R. (2015). Conservation policy and the measurement of forests. *Nature Climate Change, 6*, 192-196

Sexton, J.O., Song, X.-P., Feng, M., Noojipady, P., Anand, A., Huang, C., Kim, D.-H., Collins,

675   K.M., Channan, S., DiMiceli, C., & Townshend, J.R. (2013a). Global, 30-m resolution continuous fields of tree cover: Landsat-based rescaling of MODIS vegetation continuous fields with lidar-based estimates of error. *International Journal of Digital Earth, 6*, 427-448

Sexton, J.O., Song, X.P., Feng, M., Noojipady, P., Anand, A., Huang, C.Q., Kim, D.H., Collins, K.M., Channan, S., DiMiceli, C., & Townshend, J.R. (2013b). Global, 30-m resolution continuous

680   fields of tree cover: Landsat-based rescaling of MODIS vegetation continuous fields with lidar-based estimates of error. *International Journal of Digital Earth, 6*, 427-448

Shimada, M., Itoh, T., Motooka, T., Watanabe, M., Shiraishi, T., Thapa, R., & Lucas, R. (2014). New global forest/non-forest maps from ALOS PALSAR data (2007-2010). *Remote Sensing of Environment, 155*, 13-31

685   Smith, W.B., Lara, R.A.C., Caballero, C.E.D., Valdivia, C.I.G., Kapron, J.S., Reyes, J.C.L., Tovar, C.L.M., Miles, P.D., Oswalt, S.N., & Salgado, M.R. (2018). The North American Forest Database: going beyond national-level forest resource assessment statistics. *Environmental Monitoring and Assessment, 190*, 350

Soh, W.K., Yiotis, C., Murray, M., Parnell, A., Wright, I.J., Spicer, R.A., Lawson, T., Caballero,

690   R., & McElwain, J.C. (2019). Rising CO2 drives divergence in water use efficiency of evergreen and deciduous plants. *Science Advances, 5*, eaax7906

Soudani, K., Hmimina, G., Delpierre, N., Pontailler, J.Y., Aubinet, M., Bonal, D., Caquet, B., de Grandcourt, A., Burban, B., Flechard, C., Guyon, D., Granier, A., Gross, P., Heinesh, B., Longdoz, B., Loustau, D., Moureaux, C., Ourcival, J.M., Rambal, S., Saint André, L., & Dufrêne, E. (2012).

695   Ground-based Network of NDVI measurements for tracking temporal dynamics of canopy

structure and vegetation phenology in different biomes. *Remote Sensing of Environment, 123*, 234-245

Souza, C., Firestone, L., Silva, L.M., & Roberts, D. (2003). Mapping forest degradation in the Eastern Amazon from SPOT 4 through spectral mixture models. *Remote Sensing of Environment, 87*, 494-506

Stibig, H.-J., & Malingreau, J.-P. (2003). Forest cover of insular Southeast Asia mapped from recent satellite images of coarse spatial resolution. *AMBIO: A Journal of the Human Environment, 32*, 469-475

Stibig, H.J., Achard, F., & Fritz, S. (2004). A new forest cover map of continental southeast Asia derived from SPOT‑VEGETATION satellite imagery. *Applied Vegetation Science, 7*, 153-162

Tang, H., Armston, J., Hancock, S., Marselis, S., Goetz, S., & Dubayah, R. (2019). Characterizing global forest canopy cover distribution using spaceborne lidar. *Remote Sensing of Environment, 231*, 111262

Tchuenté, A.T.K., Roujean, J.-L., & De Jong, S.M. (2011). Comparison and relative quality assessment of the GLC2000, GLOBCOVER, MODIS and ECOCLIMAP land cover data sets at the African continental scale. *International Journal of Applied Earth Observation and Geoinformation, 13*, 207-219

Thapa, R.B., Itoh, T., Shimada, M., Watanabe, M., Takeshi, M., & Shiraishi, T. (2014). Evaluation of ALOS PALSAR sensitivity for characterizing natural forest cover in wider tropical areas. *Remote Sensing of Environment, 155*, 32-41

Tran, T.V., de Beurs, K.M., & Julian, J.P. (2016). Monitoring forest disturbances in Southeast Oklahoma using Landsat and MODIS images. *International Journal of Applied Earth Observation and Geoinformation, 44*, 42-52

Twidwell, D., West, A.S., Hiatt, W.B., Ramirez, A.L., Winter, J.T., Engle, D.M., Fuhlendorf, S.D., & Carlson, J. (2016). Plant invasions or fire policy: which has altered fire behavior more in tallgrass prairie? *Ecosystems, 19*, 356-368

Vermote, E., Justice, C., Claverie, M., & Franch, B. (2016). Preliminary analysis of the performance of the Landsat 8/OLI land surface reflectance product. *Remote Sensing of Environment, 185*, 46-56

Zhang, Y., Ling, F., Foody, G.M., Ge, Y., Boyd, D.S., Li, X., Du, Y., & Atkinson, P.M. (2019). Mapping annual forest cover by fusing PALSAR/PALSAR-2 and MODIS NDVI during 2007–2016. *Remote Sensing of Environment, 224*, 74-91